CHEMISTRY OF MATERIALS
Article

Chem. Mater. **XXXX,** *XXX,* 000–000 A
DOI:10.1021/cm9036988

Efficient Dye-Sensitized Solar Cells with an Organic Photosensitizer Featuring Orderly Conjugated Ethylenedioxythiophene and Dithienosilole Blocks

Wangdong Zeng,[†,‡] Yiming Cao,[†] Yu Bai,[†] Yinghui Wang,[†] Yushuai Shi,[†] Min Zhang,[†] Fangfang Wang,[†] Chunyue Pan,[‡] and Peng Wang*[,†]

[†]*State Key Laboratory of Polymer Physics and Chemistry, Changchun Institute of Applied Chemistry, Chinese Academy of Sciences, Changchun 130022, China and* [‡]*College of Chemistry and Chemical Engineering, Central South University, Changsha 410083, China*

Received December 8, 2009. Revised Manuscript Received December 20, 2009

In view of the limited ruthenium resource, metal-free organic dyes may play a prominent role in the coming large-scale application of cost-effective dye-sensitized solar cells, if their efficiency and stability can be considerably improved. In this paper we utilized a binary π-conjugated spacer of ethylenedioxythiophene and dithienosilole to construct a high molar absorption coefficient push−pull dye, characteristic of an intramolecular charge-transfer band peaking at 584 nm measured in chloroform. In comparison with the standard ruthenium sensitizer **Z907**, this metal-free chromophore **C219** endowed a nanocrystalline titania film with an evident light-harvesting enhancement, leading to an unprecedented 10.0−10.3% efficiency at the AM1.5G conditions for dye-sensitized solar cells with nonruthenium dyestuffs, although a highly volatile electrolyte was used. Transient absorption measurements have revealed that even if the kinetics of back-electron transfer and dye regeneration are considerably different for **Z907** and **C219**, the branching ratios of these two charge-transfer channels are over 35 for both dyes, ensuring a high yield of net charge separation at the titania/dye/electrolyte interface. A solvent-free ionic liquid cell with **C219** as the sensitizer exhibited an impressive efficiency of 8.9% under a low light intensity of 14.39 mW cm^{-2}, making it very favorable for the indoor application of flexible dye-sensitized solar cells.

1. Introduction

Photovoltaic cells have great potential for a low-carbon energy supply but so far remain expensive relative to other technologies. Greatly increased penetration of solar cells into global energy markets requires an expansion in attention from designs of high efficiency devices to those that can deliver significantly lower cost per kilowatt-hour.[1] In the past years, tremendous research efforts have been devoted to dye-sensitized solar cells[2] (DSCs) during the surging on cost-effective and resource-unlimited photovoltaic technologies. It is also valuable to note that the production of DSC key materials are more environmentally friendly and energy-saving in contrast to the traditional silicon technology. The foremost feature of DSCs consists in a nanoporous semiconducting film grafted with light-harvesting dye molecules, which could be either immersed in a redox electrolyte or filled by a hole-transporter. This charming assembly of low-cost materials can perform the functions of light absorption, charge generation, and charge transport, efficiently converting light energy to electricity. On the basis of continuous material innovation and device engineering, a state of the art DSC has achieved a validated efficiency of 11.1% measured at the AM1.5G conditions, albeit the utilization of a highly volatile electrolyte.[3]

With a view to the limited ruthenium resource, metal-free organic dyes have attracted considerable attention in recent years owing to their excellent flexibility in terms of molecular tailoring. In this regard, enormous studies have been focused on energy-level engineering of chromophores to attain a capability of panchromatic light-harvesting.[4] Furthermore, these dyestuffs need to be controllably grafted onto a nanostructured semiconducting film with favorable stacking modes and energy alignments, which have significant influences on multichanel charge-transfer kinetics, determing the ultimate cell efficienies. In this contribution, we report a very promising sensitizer coded **C219** and presented in Figure 1. A distinguishable feature of this amphiphilic push−pull chromophore consists in a binary π-conjugated spacer, apart from the blocks of a lipophilic alkoxy-substituted triphenylamine electron-donor (D) and a hydrophilic cyanoacrylic acid electron-acceptor (A). Here electron-rich 3,4-ethylenedioxythiophene unit (EDOT) is connected to D to lift up the highest occupied molecular

*To whom correspondence should be addressed. E-mail: peng.wang@ciac.jl.cn.

(1) Wadia, C.; Alivisatos, A. P.; Kammen, D. M. *Environ. Sci. Technol.* **2009**, *43*, 2072.
(2) O'Regan, B.; Grätzel, M. *Nature* **1991**, *353*, 737.
(3) Chiba, Y.; Islam, A.; Watanabe, Y.; Komiya, R.; Koide, N.; Han, L. *Jpn. J. Appl. Phys.* **2006**, *45* (Part 2), L638.

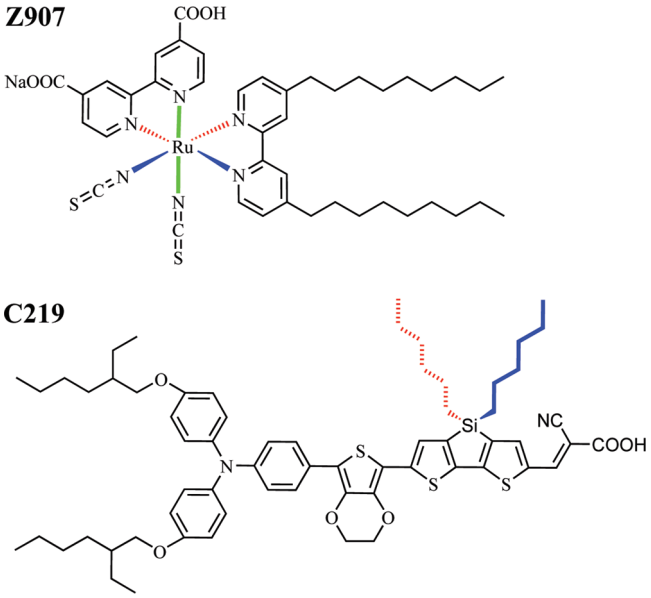

Figure 1. Molecular structures of **Z907** and **C219**.

orbital (HOMO) properly, and dihexyl-substituted dithienosilole (DTS)[5] conjugated with A keeps a suitable lowest unoccupied molecular orbital (LUMO). This is the first time that DTS has been used in the design of photosensitizers in DSCs. Moreover, the introduction of dihexyl-substituted DTS featuring a tetrahedral silicon center will not affect the planarity of π-conjugated spacer but may significantly reduce the $\pi-\pi$ stacking of dye molecules on nanocrystals. An aggregation of dye molecules on nanocrystals may lead to a dissipative intermolecular charge transfer, which could have an adverse effect on the cell efficiency.[4o,6] Even with a preliminary optimization this novel photosensitizer **C219** has already achieved a strikingly high efficiency of 10.0−10.3% measured under irradiation of AM1.5G full sunlight, in contrast to 9.3% attained with the standard amphiphilic ruthenium dye **Z907** (Figure 1).

2. Experimental Section

2.1. Materials. All solvents and reagents, unless otherwise stated, were of puriss quality and used as received. *n*-Butyllithium, 2-cyanoacetic acid, guanidinium thiocyanate (GNCS), *tert*-butylpyridine (TBP), and 3α,7α-dihyroxy-5*β*-cholic acid (cheno) were purchased from Fluka. 3,3′-Di-*n*-hexylsilylene-2,2′-bithiophene (**1**),[7] 1-(2-ethylhexyloxy)-4-iodobenzene (**4**),[8] 2-(tributylstannyl)-3,4-(ethylenedioxy)thiophene,[9] and **Z907**[10] were synthesized according to the corresponding literature methods. The synthesis of 1,3-dimethylimidazolium iodide (DMII) and 1-ethyl-3-methylimidazolium iodide (EMII) was described in our previous paper.[11] The scattering TiO_2 paste (WER2-O) and 1-ethyl-3-methylimidazolium tetracyanoborate (EMITCB) were received as gifts from Dyesol. The synthetic route of **C219** is outlined in Scheme 1 and the details are described as follows.

Synthesis of 3,3′-Di-n-hexylsilylene-2,2′-bithiophene-5-carbaldehyde (*2*). To a cold solution of **1** (1.46 g, 4.03 mmol) and *N*,*N*-dimethylformide (0.35 g, 4.84 mmol) in 1,2-dichloroethane (10 mL) at 0 °C was added phosphorus chloride oxide (0.74 g, 4.84 mmol). The reaction solution was heated to 80 °C, stirred for 4 h, and then saturated sodium acetate aqueous solution (20 mL) added. The mixture was further stirred at room temperature for 30 min. The crude product was extracted into dichloromethane, and the organic layer was washed with brine and water, and dried over anhydrous sodium sulfate. After removing solvent under reduced pressure, the residue was purified by column chromatography (dichloromethane/petroleum ether 60−90 °C, 2/1, *v*/*v*) on silica gel to yield a colorless oil (96% yield). ^{1}H NMR (600 MHz, DMSO-d_6) δ: 9.87 (s, 1H), 8.05 (s, 1H), 7.41 (d, J = 4.8 Hz, 1H), 7.12 (d, J = 4.8 Hz, 1H), 1.30 (m, 4H), 1.21 (m, 4H), 1.16 (m, 8H), 0.95 (t, J = 6.8 Hz, 4H), 0.78 (t, J = 6.8 Hz, 6H). ^{13}C NMR (150 MHz, DMSO-d_6) δ: 183.73, 156.85, 146.86, 146.58, 144.06, 142.81, 141.18, 130.63,

(4) For example, see: (a) Hara, K.; Kurashige, M.; Dan-oh, Y.; Kasada, C.; Shinpo, A.; Suga, S.; Sayama, K.; Arakawa, H. *New J. Chem.* **2003**, *27*, 783. (b) Kitamura, T.; Ikeda, M.; Shigaki, K.; Inoue, T.; Anderson, N. A.; Ai, X.; Lian, T.; Yanagida, S. *Chem. Mater.* **2004**, *16*, 1806. (c) Horiuchi, T.; Miura, H.; Sumioka, K.; Uchida, S. *J. Am. Chem. Soc.* **2004**, *126*, 12218. (d) Thomas, K. R. J.; Lin, J. T.; Hsu, Y.-C.; Ho, K.-C. *Chem. Commun.* **2005**, 4098. (e) Chen, Y.; Zeng, Z.; Li, C.; Wang, W.; Wang, X.; Zhang, B. *New. J. Chem.* **2005**, *29*, 773. (f) Hagberg, D. P.; Edvinsson, T.; Marinado, T.; Boschloo, G.; Hagfeldt, A.; Sun, L. *Chem. Commun.* **2006**, 2245. (g) Li, S.-L.; Jiang, K.-J.; Shao, K.-F.; Yang, L.-M. *Chem. Commun.* **2006**, 2792. (h) Koumura, N.; Wang, Z.-S.; Mori, S.; Miyashita, M.; Suzuki, E.; Hara, K. *J. Am. Chem. Soc.* **2006**, *128*, 14256. (i) Kim, S.; Lee, J. W.; Kang, S. O.; Ko, J.; Yum, J.-H.; Fantacci, S.; De Angellis, F.; Di Censo, D.; Nazeeruddin, M. K.; Grätzel, M. *J. Am. Chem. Soc.* **2006**, *128*, 16701. (j) Wang, Z.-S.; Cui, Y.; Hara, K.; Dan-oh, Y.; Kasada, C.; Shinpo, A. *Adv. Mater.* **2007**, *19*, 1138. (k) Edvinsson, T.; Li, C.; Pschirer, N.; Schöneboom, J.; Eickemeyer, F.; Sens, R.; Boschloo, G.; Herrmann, A.; Müllen, K.; Hagfeldt, A. *J. Phys. Chem. C* **2007**, *111*, 15137. (l) Ito, S.; Miura, H.; Uchida, S.; Takata, M.; Sumioka, K.; Liska, P.; Comte, P.; Péchy, P.; Grätzel, M. *Chem. Commun.* **2008**, 5194. (m) Thomas, K. R. J.; Hsu, Y.-C.; Lin, J. T.; Lee, K.-M.; Ho, K.-C.; Lai, C.-H.; Cheng, Y.-M.; Chou, P.-T. *Chem. Mater.* **2008**, *20*, 1830. (n) Zhou, G.; Pschirer, N.; Schöneboom, J. C.; Eickemeyer, F.; Baumgarten, M.; Müllen, K. *Chem. Mater.* **2008**, *20*, 1808. (o) Wang, Z.-S.; Koumura, N.; Cui, Y.; Takahashi, M.; Sekiguchi, H.; Mori, A.; Kubo, T.; Furube, A.; Hara, K. *Chem. Mater.* **2008**, *20*, 3993. (p) Lin, J. T.; Chen, P.-C.; Yen, Y.-S.; Hsu, Y.-C.; Chou, H.-H.; Yeh, M.-C. P. *Org. Lett.* **2009**, *11*, 97. (q) Tian, H.; Yang, X.; Cong, J.; Chen, R.; Liu, J.; Hao, Y.; Hagfeldt, A.; Sun, L. *Chem. Commun.* **2009**, 6288. (r) Tian, H.; Yang, X.; Chen, R.; Hagfeldt, A.; Sun, L. *Energy Environ. Sci.* **2009**, *2*, 674. (s) Teng, C.; Yang, X.; Yuan, C.; Li, C.; Chen, R.; Tian, H.; Li, S.; Hagfeldt, A.; Sun, L. *Org. Lett.* **2009**, *11*, 5542. (t) Kumaresan, D.; Thummel, R. P.; Bura, T.; Ulrich, G.; Ziessel, R. *Chem.—Eur. J.* **2009**, *15*, 6335. (u) Wang, Z.-S.; Koumura, N.; Cui, Y.; Miyashita, M.; Mori, S.; Hara, K. *Chem. Mater.* **2009**, *21*, 2810. (v) Song, J.; Zhang, F.; Li, C.; Liu, W.; Li, B.; Huang, Y.; Bo, Z. *J. Phys. Chem. C* **2009**, *113*, 13391. (w) Preat, J.; Michaux, C.; Jacquemin, D.; Perpète, E. A. *J. Phys. Chem. C* **2009**, *113*, 16821. (x) Li, Q.; Lu, L.; Zhong, C.; Shi, J.; Huang, Q.; Jin, X.; Peng, T.; Qin, J.; Li, Z. *J. Phys. Chem. B* **2009**, *113*, 14588. (y) Liu, B.; Zhu, W.; Zhang, Q.; Wu, W.; Xu, M.; Ning, Z.; Xie, Y.; Tian, H. *Chem. Commun.* **2009**, 1766 and references cited therein. (z) Mishra, A.; Fischer, M. K. R.; Bäuerle, P. *Angew. Chem., Int. Ed.* **2009**, *48*, 2474 and references cited therein.
(5) (a) Ohshita, J. *Macromol. Chem. Phys.* **2009**, *210*, 1360. (b) Zhan, X.; Barlow, S.; Marder, S. R. *Chem. Commun.* **2009**, 1948.
(6) Wang, X.-F.; Kitao, O.; Zhou, H.; Tamiaki, H.; Sasaki, S.-i. *J. Phys. Chem. C* **2009**, *113*, 7954.
(7) (a) Lu, G.; Usta, H.; Risko, C.; Wang, L.; Facchetti, A.; Ratner, M. A.; Marks, T. J. *J. Am. Chem. Soc.* **2008**, *130*, 7670. (b) Hou, J. H.; Chen, H.- Y.; Zhang, S. Q.; Li, G.; Yang, Y. *J. Am. Chem. Soc.* **2008**, *130*, 16144. (c) Beaujuge, P. M.; Pisula, W.; Tsao, H. N.; Ellinger, S.; Müllen, K.; Reynolds, J. R. *J. Am. Chem. Soc.* **2009**, *131*, 7514. (d) Huo, L.; Chen, H.-Y.; Hou, J.; Chen, T. L.; Yang, Y. *Chem. Commun.* **2009**, 5570.
(8) Hiroko, Y.; Ikuyoshi, T.; Kazuchika, O.; Takeshi, E. *Mol. Cryst. Liq. Cryst. A* **2001**, *369*, 47.
(9) Zhu, S. S.; Swager, T. M. *J. Am. Chem. Soc.* **1997**, *119*, 12568.
(10) Wang, P.; Wenger, B.; Humphry-Baker, R.; Moser, J.-E.; Teuscher, J.; Kantlehner, W.; Mezger, J.; Stoyanov, E. V.; Zakeeruddin, S. M.; Grätzel, M. *J. Am. Chem. Soc.* **2005**, *127*, 6850.
(11) Cao, Y.; Zhang, J.; Bai, Y.; Li, R.; Zakeeruddin, S. M.; Grätzel, M.; Wang, P. *J. Phys. Chem. C* **2008**, *112*, 13775.

Scheme 1. Synthetic Route of the C219 Dye[a]

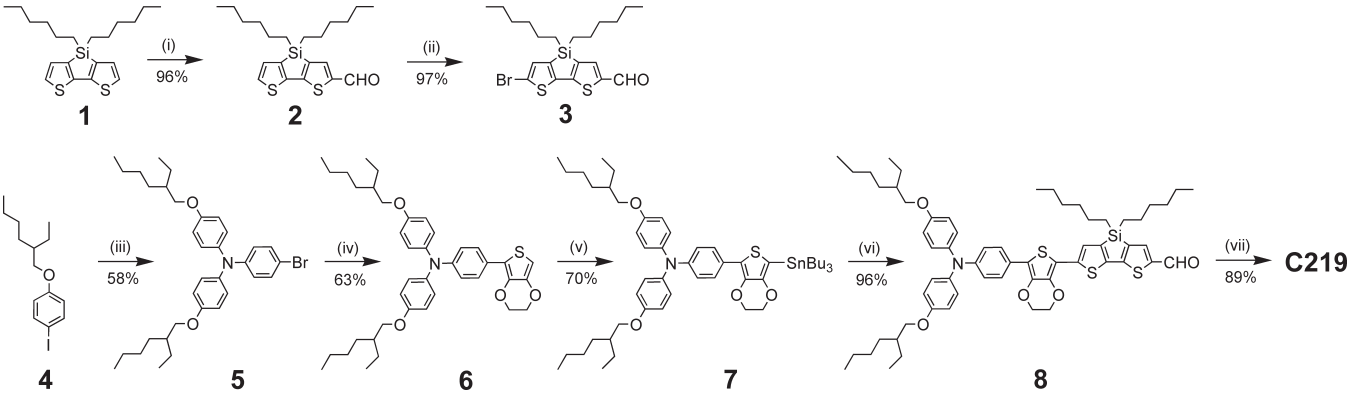

[a] Reagents: (i) $POCl_3$, DMF, 1,2-dichloroethane; (ii) NBS, DMF; (iii) 4-bromoaniline, CuCl, 1,10-phenathroline, KOH, toluene; (iv) 2-(tributylstannyl)-3,4-(ethylenedioxy)thiophene, $Pd(PPh_3)_2Cl_2$, toluene; (v) *n*-BuLi, tributylstannyl chloride, THF; (vi) **3**, $Pd(PPh_3)_2Cl_2$, toluene; (vii) cyanoacetic acid, piperidine, $CHCl_3$.

130.24, 31.85, 30.70, 23.43, 21.84, 13.80, 10.91. MS (ESI) *m*/*z* calcd for $C_{21}H_{30}OS_2Si$: 390.15. Found: 391.20 ($[M+H]^+$). Anal. Calcd for $C_{21}H_{30}OS_2Si$: C, 64.56; H, 7.74. Found: C, 64.57; H, 7.71.

Synthesis of 5′-Bromo-3,3′-di-n-hexylsilylene-2,2′-bithiophene-5-carbaldehyde (***3***). To a cold solution of **2** (1.50 g, 3.84 mmol) in *N*,*N*-dimethylformide (30 mL) was added *N*-bromosuccinimide (0.77 g, 4.33 mmol) at 0 °C under argon. The reaction mixture was warmed to room temperature, stirred for 4 h, and then water (50 mL) added. The crude product was extracted into dichloromethane, and the organic layer was dried over anhydrous sodium sulfate. After removing solvent under reduced pressure, the residue was purified by column chromatography (dichloromethane/petroleum ether 60−90 °C, 2/1, *v*/*v*) on silica gel to yield a yellowish oil (97% yield). ^{1}H NMR (600 MHz, DMSO-d_6) δ: 9.89 (s, 1H), 8.07 (s, 1H), 7.43 (s, 1H), 1.31 (m, 4H), 1.22 (m, 4H), 1.17 (m, 8H), 0.96 (t, J = 6.8 Hz, 4H), 0.79 (t, J = 6.8 Hz, 6H). ^{13}C NMR (150 MHz, DMSO-d_6) δ: 183.90, 155.64, 147.41, 147.32, 144.54, 142.17, 140.95, 133.67, 114.74, 31.83, 30.65, 23.30, 21.85, 13.80, 10.73. MS (ESI) *m*/*z* calcd for $C_{21}H_{29}BrOS_2Si$: 468.06. Found: 469.10 ($[M+H]^+$). Anal. Calcd for $C_{21}H_{29}BrOS_2Si$: C, 53.71; H, 6.22. Found: C, 53.73; H, 6.25.

Synthesis of 4-Bromo-N,N-bis((4-(2-ethyl)hexyloxy)phenyl)-aniline (***5***). To a stirred solution of **4** (70.00 g, 210.70 mmol), 4-bromoaniline (14.50 g, 84.28 mmol), and 1,10-phenanthroline (3.03 g, 16.85 mmol) in toluene (350 mL) at 100 °C were added potassium hydroxide (37.83 g, 674.24 mmol) and cuprous chloride (1.67 g, 16.85 mmol) under argon. The reaction mixture was refluxed at 120 °C overnight and water (200 mL) added. The crude product was extracted into dichloromethane, and the organic layer was washed with water and dried over anhydrous sodium sulfate. After removing solvent under reduced pressure, the residue was purified by column chromatography (ethyl acetate/petroleum ether 60−90 °C, 1/30, *v*/*v*) on silica gel to yield a yellowish oil (58% yield). ^{1}H NMR (600 MHz, DMSO-d_6) δ: 7.30 (d, J = 8.0 Hz, 2H), 7.01 (d, J = 8.0 Hz, 4H), 6.91 (d, J = 8.0 Hz, 4H), 6.65 (d, J = 8.0 Hz, 2H), 3.82 (t, J = 4.0 Hz, 4H), 1.66 (m, 2H), 1.42 (m, 8H), 1.30 (m, 8H), 0.88 (m, 12H). ^{13}C NMR (150 MHz, DMSO-d_6) δ: 155.65, 147.85, 139.46, 131.61, 126.83, 120.62, 115.53, 110.80, 70.08, 38.68, 29.90, 28.41, 23.28, 22.46, 13.09, 10.88. MS (ESI) *m*/*z* calcd for $C_{34}H_{46}BrNO_2$: 579.27. Found: 580.25 ($[M+H]^+$). Anal. Calcd for $C_{34}H_{46}BrNO_2$: C, 70.33; H, 7.99; N, 2.41. Found: C, 70.32; H, 7.89; N, 2.40.

Synthesis of 4-(3,4-Ethylenedioxythiophene-5-yl)-N,N-bis-(4-(2-ethylhexyloxy)phenyl)aniline (***6***). A mixture of **5** (9.60 g, 16.55 mmol), 2-(tributylstannyl)-3,4-(ethylenedioxy)thiophene (10.70 g, 24.82 mmol), $Pd(PPh_3)_2Cl_2$ (1.16 g, 1.65 mmol) and 150 mL of anhydrous toluene was refluxed for 16 h under argon. The crude product was extracted into dichloromethane, and the organic layer was washed with water and dried over anhydrous sodium sulfate. After removing solvent under reduced pressure, the residue was purified by column chromatography (dichloromethane/petroleum ether 60−90 °C, 1/25, *v*/*v*) on silica gel to yield a yellow oil (63% yield). ^{1}H NMR (600 MHz, DMSO-d_6) δ: 7.44 (d, J = 8.8 Hz, 2H), 6.99 (d, J = 8.8 Hz, 4H), 6.90 (d, J = 8.8 Hz, 4H), 6.79 (d, J = 8.8 Hz, 2H), 6.48 (s, 1H), 4.26 (m, 2H), 4.24 (m, 2H), 3.82 (t, J = 6.0 Hz, 4H), 1.66 (m, 2H), 1.40 (m, 8H), 1.30 (m, 8H), 0.89 (m, 12H). ^{13}C NMR (150 MHz, DMSO-d_6) δ: 155.16, 146.73, 141.90, 139.77, 137.05, 126.12, 126.04, 124.70, 119.63, 116.02, 115.32, 96.05, 70.31, 64.32, 63.86, 38.60, 29.76, 28.18, 23.18, 22.09, 13.44, 10.57. MS (ESI) *m*/*z* calcd for $C_{40}H_{51}NO_4S$: 641.35. Found: 642.35 ($[M+H]^+$). Anal. Calcd for $C_{40}H_{51}NO_4S$: C, 74.84; H, 8.01. Found: C, 74.88; H, 8.04.

Synthesis of 5′-{2-{4-[N,N-Bis(4-(2-ethylhexyloxy)phenyl)-amino]phenyl}-3,4-ethylenedioxythiophene-5-yl}-3,3′-di-n-hexylsilylene-2,2′-bithiophene-5-carbaldehyde (***8***). Compound **6** (2.00 g, 3.11 mmol) dissolved in 15 mL of anhydrous THF was treated dropwise with *n*-butyllithium (1.6 M, 2.13 mL, 3.42 mmol) at −78 °C under argon. The solution was stirred at −78 °C for 1 h and tributylstannyl chloride (1.32 g, 4.04 mmol) added. The mixture was warmed to room temperature and stirred for 6 h. The reaction was terminated by adding water and the mixture was extracted with dichloromethane and dried over anhydrous sodium sulfate. The solvent was evaporated to obtain the crude **7** as a brown oil and used in the further reaction. The 70% yield of **7** was roughly estimated according to ^{1}H NMR data. To a solution of **7** (1.01 g, 1.09 mmol) and **3** (0.87 g, 1.86 mmol) in toluene (20 mL), $Pd(PPh_3)_2Cl_2$ (0.13 g, 0.18 mmol) was added. The mixture was refluxed at 110 °C for 14 h under argon. The crude compound was extracted into ethyl acetate, washed with brine and water, and dried over anhydrous sodium sulfate. After removing solvent under reduced pressure, the residue was purified by column chromatography (ethyl acetate/petroleum ether 60−90 °C, 1:10, *v*/*v*) on silica gel to yield a red powder (96% yield). ^{1}H NMR (600 MHz, DMSO-d_6) δ: 9.86 (s, 1H), 7.99 (s, 1H), 7.49 (d, J = 8.4 Hz, 2H), 7.32 (s, 1H), 7.03

(d, J = 9.0 Hz, 4H), 6.91 (d, J = 9.0 Hz, 4H), 6.81 (d, J = 8.4 Hz, 2H), 4.44 (m, 2H), 4.37 (m, 2H), 3.85 (t, J = 6.6 Hz, 4H), 1.69 (m, 2H), 1.42 (m, 8H), 1.33 (m, 12H), 1.24 (m, 4H), 1.19 (m, 8H), 0.99 (m, 4H), 0.91 (m, 12H), 0.81 (t, J = 6.6 Hz, 6H). ^{13}C NMR (150 MHz, DMSO-d_6) δ: 182.82, 156.73, 155.39, 147.22, 144.30, 143.66, 142.02, 140.31, 139.50, 138.71, 138.43, 137.20, 126.35, 126.26, 124.97, 123.46, 119.13, 115.39, 114.97, 106.89, 70.34, 64.81, 64.34, 38.59, 31.43, 30.35, 29.74, 28.17, 23.17, 23.07, 22.06, 21.47, 13.42, 13.35, 10.70, 10.56. MS (ESI) m/z calcd for $C_{61}H_{79}NO_5S_3Si$: 1029.49. Found: 1030.50 ([M+H]$^+$). Anal. Calcd for $C_{61}H_{79}NO_5S_3Si$: C, 71.09; H, 7.73; N, 1.36. Found: C, 71.11; H, 7.75; N, 1.34.

Synthesis of 2-Cyano-3-{5′-{2-{4-[N,N-bis(4-(2-ethylhexyloxy)-phenyl)amino]phenyl}-3,4-ethylenedioxythiophene-5-yl}-3,3′-di-n-hexylsilylene-2,2′-bithiophene-5-yl}acrylic Acid (***C219***). To a stirred solution of compound **8** (1.06 g, 1.03 mmol) and cyanoacetic acid (0.26 g, 3.09 mmol) in chloroform (30 mL) was added piperidine (0.61 g, 7.21 mmol). The reaction mixture was refluxed under argon for 12 h and then acidified with 2 M hydrochloric acid aqueous solution (40 mL). The crude product was extracted into chloroform, washed with water, and dried over anhydrous sodium sulfate. After removing solvent under reduced pressure, the residue was purified by flash chromatography with chloroform and methanol/chloroform (1/10, v/v) in turn as eluent to yield a purple powder (89%). ^{1}H NMR (600 MHz, DMSO-d_6) δ: 13.49 (s, 1H), 8.45 (s, 1H), 8.00 (s, 1H), 7.48 (d, J = 8.8 Hz, 2H), 7.34 (s, 1H), 7.00 (d, J = 8.8 Hz, 4H), 6.90 (d, J = 8.8 Hz, 4H), 6.78 (d, J = 8.8 Hz, 2H), 4.44 (m, 2H), 4.37 (m, 2H), 3.82 (d, J = 5.2 Hz, 4H), 1.66 (m, 2H), 1.42 (m, 16H), 1.22 (m, 16H), 0.97 (m, 4H), 0.90 (m, 12H), 0.78 (t, J = 6.4 Hz, 6H). ^{13}C NMR (150 MHz, DMSO-d_6) δ: 163.98, 158.37, 155.50, 147.92, 147.37, 146.56, 144.42, 143.20, 142.09, 139.53, 139.38, 139.16, 137.38, 136.38, 126.67, 126.48, 125.20, 123.44, 119.16, 117.01, 115.45, 107.06, 95.12, 70.08, 65.10, 64.57, 38.69, 31.86, 30.69, 29.90, 28.41, 23.37, 23.29, 22.45, 21.86, 13.87, 13.80, 10.87. ATR-FTIR: 1680 cm^{-1} (COOH), 2214 cm^{-1} (CN). MS (ESI) m/z calcd for $C_{64}H_{80}N_2O_6S_3Si$: 1096.49. Found: 1097.61 ([M+H]$^+$). Anal. Calcd for $C_{64}H_{80}N_2O_6S_3Si$: C, 70.03; H, 7.35; N, 2.55. Found: C, 70.02; H, 7.36; N, 2.54.

2.2. Device Fabrication. A screen-printed single or double layer film of interconnected titania particles was used as the negative electrode. A transparent layer of 20-nm-sized titania particles was first printed on the fluorine-doped SnO_2 (FTO, Nippon Sheet Glass, Solar, 4 mm thick) conducting glass electrode and further coated by a second layer of scattering titania particles if needed. The film thickness was measured by a benchtop Ambios XP-1 stylus profilometer. The detailed preparation procedures of titania nanocrystals, pastes for screen-printing, and nanostructured titania films have been reported in a previous paper.[12] A cycloidal titania electrode (~0.28 cm^2) was stained by immersing it into a dye solution (150 μM **C219** and 300 μM cheno in chlorobenzene, 3−4 h; 300 μM **Z907** and 300 μM cheno in the 1:1 mixture of acetonitrile and *tert*-butanol, overnight). After washing with acetonitrile and drying by air flow, the dye-coated titania electrode was assembled with a thermally platinized FTO (TEC 15 Ω/□, Libbey-Owens-Ford Industries, 2.2 mm thick) electrode. The electrodes were separated by a 30-μm-thick Bynel (DuPont) hot-melt gasket and sealed up by heating. The internal space was filled with a liquid electrolyte using a vacuum backfilling system. The electrolyte-injecting hole on the counter electrode glass substrate made with a sand-blasting drill, was sealed with a Bynel sheet and a thin glass cover by heating. Two electrolytes were used for device evaluations. **EL01**: 1.0 M DMII, 50 mM LiI, 30 mM I_2, 0.5 M TBP, and 0.1 M GNCS in the 85/15 mixture of acetonitrile and valeronitrile; **EL02**: DMII/EMII/EMITCB/I_2/TBP/GNCS (molar ratio: 12/12/16/1.67/3.33/0.67), where the iodide and triiodide concentrations are 3.18 and 0.24 M, respectively.

2.3. Calculation. The ground-state geometry of **C219** was fully optimized by the density functional theory (DFT) method[13] with Beck's three-parameter functional and Lee−Yang−Parr functional[14] (B3LYP) and the 6-31G basis set was used for all atoms.[15] The electronic transitions were calculated by time-dependent density functional theory (TDDFT) method[16] based on the optimized ground-state structure. All calculations were performed with the Gaussian03 program package.

2.4. UV−Vis, Voltammetric, Photoluminescence, and Transient Absorption Measurements. Electronic absorption spectra were recorded on a UNICO WFZ UV-2802PC/PCS spectrometer. A CHI660C electrochemical workstation was used for square-wave voltammetric measurements in combination with a mini three-electrode electrochemical cell equipped with a 5-μm-radius Pt ultramicroelectrode as working electrode. A Pt wire and a silver wire were used as counter and quasi-reference electrodes, respectively. The redox potentials were calibrated with ferrocene as the internal reference. Photoluminescence spectra and decays were measured with a LifeSpec-II fluorescence spectrometer equipped with an EPL405 laser diode. Transient absorption measurements were carried out with a LP920 laser flash spectrometer in conjunction with a nanosecond tunable OPOLett-355II laser. The sample was kept at a 45° angle to the excitation beam. The probe light from a pulsed xenon arc lamp was passed through various optical elements, samples, and a monochromator before being detected by a fast photomultiplier tube and recorded with a TDS 3012C digital signal analyzer.

2.5. Photovoltaic Measurements and Stability Tests. A Keithley 2400 source meter and a Zolix Omni-λ300 monochromator equipped with a 500 W xenon lamp were used to measure photocurrent action spectra, with a wavelength sampling interval of 10 nm and a current sampling time of 2 s under the full computer control. Monochromatic incident photon-to-collected electron conversion efficiency (IPCE) is defined by IPCE-(λ) = $hcJ_{sc}/e\phi\lambda$, where h is the Planck constant, c is the light speed in vacuum, e is the electronic charge, λ is the wavelength, J_{sc} is the short-circuit photocurrent density, and ϕ is the incident radiative flux. A Hamamatsu S1337−1010BQ silicon diode used for IPCE measurements was calibrated in National Institute of Metrology, China. A model LS1000-4S-AM1.5G-1000W solar simulator (Solar Light Company, USA) in combination with a metal mesh was employed to give an irradiance of 100 mW cm^{-2}. The light intensity was tested with a PMA2144 pyranometer and a calibrated PMA 2100 dose control system. $J-V$ characteristics were obtained by applying a bias potential to a testing cell and measuring dark current and photocurrent with a Keithley 2602 source meter under the full computer control. The measurements were fully automated using Labview 8.0. A metal mask with an aperture area of 0.158 cm^2 was covered on a testing

(12) Wang, P.; Zakeeruddin, S. M.; Comte, P.; Charvet, R.; Humphry-Baker, R.; Grätzel, M. *J. Phys. Chem. B* **2003**, *107*, 14336.

(13) Runge, E.; Gross, E. K. U. *Phys. Rev. Lett.* **1984**, *52*, 997.
(14) (a) Becke, A. D. *J. Chem. Phys.* **1993**, *98*, 5648. (b) Lee, C.; Yang, W.; Parr, R. G. *Phys. Rev. B* **1988**, *37*, 785.
(15) Hay, P. J.; Wadt, W. R. *J. Chem. Phys.* **1985**, *82*, 299.
(16) (a) Matsuzawa, N. N.; Ishitani, A. *J. Phys. Chem. A* **2001**, *105*, 4953. (b) Stratmann, R. E.; Scuseria, G. E. *J. Chem. Phys.* **1998**, *109*, 8218.

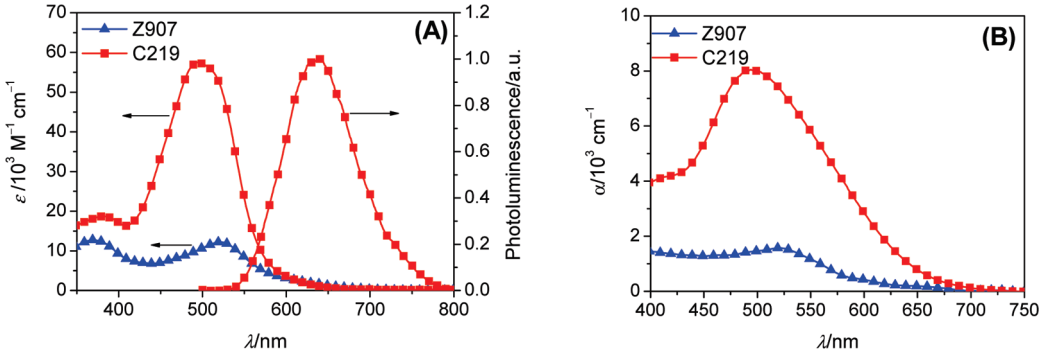

Figure 2. (**A**) Electronic absorption spectra of **Z907** and **C219** in DMF and photoluminescence spectrum of **C219** in DMF obtained with a laser excitation at 405 nm. (**B**) Absorption spectra of **Z907** and **C219** anchored on a 2.4 μm thick mesoporous titania film.

cell during all measurements. An antireflection film (λ < 380 nm, ARKTOP, ASAHI Glass) is adhered to the DSC photoanode during IPCE and $J-V$ measurements. A homemade heating−cooling system was used for temperature-dependent experiments. Solar cells covered with a 50 μm thick of polyester film (Preservation Equipment Ltd., UK) as a 400 nm UV cutoff filter were irradiated at open circuit under a Suntest CPS plus lamp (ATLAS GmbH, 100 mW cm^{-2}) in ambient air at 60 °C. $J-V$ measurements were carried out at room temperature after allowing the cells to cool down and equilibrate for 30 min.

2.6. Electrical Impedance Measurements. Electrical impedance experiments were carried out in the dark with an IM6ex electrochemical workstation, with a frequency range from 50 mHz to 100 kHz and a potential modulation of 10 mV. The obtained impedance spectra were fitted with the Z-view software (v2.80, Scribner Associates Inc.) in terms of appropriate equivalent circuits. A homemade heating−cooling system was used for temperature-dependent measurements.

2.7. Transient Photoelectrical Measurements. In transient photoelectrical decay experiments, a steady light was supplied with a white light-emitting diode (LED) array while a perturbing light pulse was provided with a red LED array controlled by a fast solid-state switch. Both white and red lights were irradiated on the photoanode side of a testing cell. The red pulse was carefully controlled by the driving potential of diodes to keep the modulated photovoltage below 5 mV. We used red light as a probe to generate a photovoltage perturbation near the open-circuit photovoltage (V_{oc}) of the cell under the white light and measured the voltage decay process thereafter. Normally, the transient signals follow a single exponential decay, therefore the recombination rate constant, k_r, can be extracted from the slope of the semilogarithmic plot. The capacitance (C_μ) of the titania interface at the V_{oc} is calculated by $C_\mu = \Delta Q/\Delta V$, where ΔV is the peak of the photovoltage transient and ΔQ is the number of electron injected during the red light flash. The latter is obtained by integrating a short-circuit photocurrent transient generated from an identical red pulse. The electron density (d_e) in the titania film under a given white light intensity was determined by charge extraction technique. A homemade heating−cooling system was used for temperature-dependent measurements.

3. Results and Discussion

3.1. Electronic Absorption and Energy Level. Distinct from photocatalytic degradation of organic pollutants realized by a direct band excitation of titania nanocrystals with high-energy photons,[17] it is pertinent to keep dye-sensitized solar cells away from irradiation of UV photons, assuring a long haul device operation. This consideration is based on our observation on an evident deterioration of cell efficiencies if UV light is not filtered. We deduce that this should be ascribed to structural modifications of dye molecules, which are probably attacked by high-energy holes in the photoexcited titania nanocrystals. In this regard, an antireflection film can be coated onto DSCs, filtering UV photons and reducing the reflection of visible photons simultaneously. Therefore, in DSCs, the sensitizer normally functions as the only light-absorption component making a contribution to the subsequent charge generation.

Therefore, we first measured the electronic absorption spectrum of **C219** dissolved in DMF to have a preliminary evaluation on its light-harvesting capacity, in comparison with the standard amphiphilic ruthenium dye **Z907**. As presented in Figure 2A, the molar extinction coefficient (ε) of 57.5 × 10^3 M^{-1} cm^{-1} at 493 nm measured for **C219** is over four times higher than that of 12.2 × 10^3 M^{-1} cm^{-1} at 521 nm for **Z907**. In view of the strong influence of solvent polarities on charge-transfer transitions of organic push−pull chromophores,[18] we further measured the absorption of **C219** in chloroform to have a systematic comparison with other metal-free photosensitizers reported in our previous work[19] and the details are collected in Table S1 of the Supporting Information. Among these dyes, the low-energy electronic transition of **C219** arises at the longest wavelength of 584 nm, demonstrating a sound advancement in terms of enhancing the near-infrared light-harvesting. More importantly, **C219** bestows significantly improved light

(17) Legrini, O.; Oliveros, E.; Braun, A. M. *Chem. Rev.* **1993**, *93*, 671.

(18) Meier, H. *Angew. Chem., Int. Ed.* **2005**, *44*, 2482.

(19) (a) Wang, M.; Xu, M.; Shi, D.; Li, R.; Gao, F.; Zhang, G.; Yi, Z.; Humphry-Baker, R.; Wang, P.; Zakeeruddin, S. M.; Grätzel, M. *Adv. Mater.* **2008**, *20*, 4460. (b) Qin, H.; Wenger, S.; Xu, M.; Gao, F.; Jing, X.; Wang, P.; Zakeeruddin, S. M.; Grätzel, M. *J. Am. Chem. Soc.* **2008**, *130*, 9202. (c) Shi, D.; Pootrakuchote, N.; Yi, Z.; Xu, M.; Zakeeruddin, S. M.; Grätzel, M.; Wang, P. *J. Phys. Chem. C* **2008**, *112*, 17478. (d) Xu, M.; Li, R.; Pootrakulchote, N.; Shi, D.; Guo, J.; Yi, Z.; Zakeeruddin, S. M.; Grätzel, M.; Wang, P. *J. Phys. Chem. C* **2008**, *112*, 19770. (e) Xu, M.; Wenger, S.; Bara, H.; Shi, D.; Li, R.; Zhou, Y.; Zakeeruddin, S. M.; Grätzel, M.; Wang, P. *J. Phys. Chem. C* **2009**, *113*, 2966. (f) Li, R.; Lv, X.; Shi, D.; Zhou, D.; Cheng, X.; Zhang, G.; Wang, P. *J. Phys. Chem. C* **2009**, *113*, 7469. (g) Zhang, G.; Bai, Y.; Li, R.; Shi, D.; Wenger, S.; Zakeeruddin, S. M.; Grätzel, M.; Wang, P. *Energy Environ. Sci.* **2009**, *2*, 92. (h) Zhang, G.; Bala, H.; Cheng, Y.; Shi, D.; Lv, X.; Yu, Q.; Wang, P. *Chem. Commun.* **2009**, 2198.

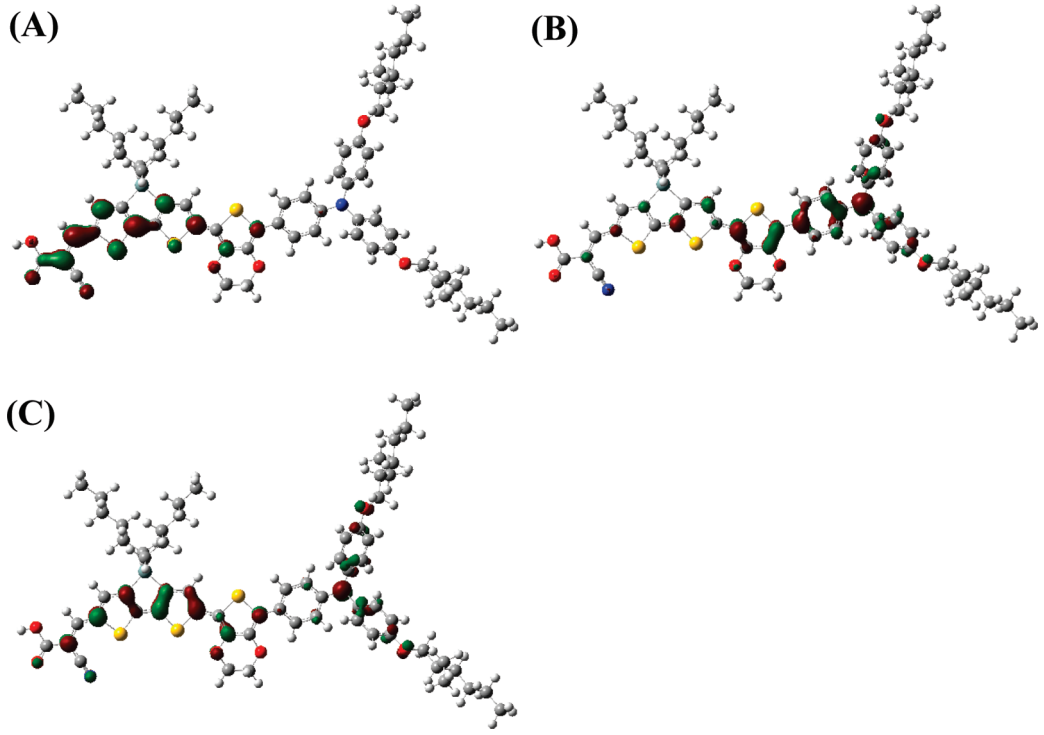

Figure 3. Contour representations of (A) LUMO, (B) HOMO, and (C) HOMO−1 of **C219**. All the iodensity surface values are fixed at 0.04.

absorption coefficients (Figure 2B) upon a titania film in contrast to **Z907**, ensuring a good light absorption even if a thin active layer must be used for efficient device operation.[19a] On the other hand, a reduction in film thickness can improve the open-circuit photovoltage, benefiting from an uplifted electron-Fermi level of a titania negative electrode because of the intensified electron density under a given light intensity.

The electronic absorption origins are scrutinized by calculating the singlet electronic transitions with the TDDFT method in Gaussian03W program suite. Calculation results show that the visible absorption of **C219** stems from the $\pi \rightarrow \pi^*$ transitions mostly from HOMO to LUMO and subsidiarily from HOMO−1 to LUMO. The isodensity surface plots of HOMO, HOMO−1, and LUMO are presented in Figure 3. HOMO of **C219** is populated over the triphenylamine, EDOT, and DTS blocks with considerable contribution from the former, whereas LUMO is delocalized through the EDOT, DTS, and cyanoacrylic acid fragments with sizable contribution from the latter. This spatially directed separation of HOMO and LUMO is an ideal condition for dye-sensitized solar cells, which not only facilitates ultrafast interfacial electron injection from excited dyes to titania but also slows down recombination of injected electrons with oxidized dye cations because of their remoteness. In addition, the hole localization on the triphenylamine fragment facilitates the electron donor to approach, promoting the fast dye regeneration. It is valuable to note that the $\sigma^*-\pi^*$-interactions typically observed for the small silole structures[5] are actually not inspected for the LUMO of **C219**, likely because of the energetic stabilization of carbon-backbone-based π^*-orbital by the strong electron-withdrawing cyanoacrylic acid fragment. Moreover, both HOMO and LUMO exhibit overlapping extension to the EDOT and DST spacers, enhancing the electronic coupling parallel to the electronic transition dipole moment between the two states, which in turn augments the oscillator strength between these two electronic states.

The DMF solution of **C219** has a strong red emission centered at 688 nm, featuring a single exponential lifetime of 1.23 ns derived from our picosecond time-correlated single photon counting (TCSPC) measurements. The excitation transition energy (E_{0-0}) was roughly estimated to be 2.19 eV from the intersection of absorption and photoluminescence spectra. The redox potentials of **Z907** and **C219** in DMF were accurately measured by employing the ultramicroelectrode technique in conjunction with square-wave voltammetry. The HOMO and LUMO values versus vacuum were transformed via the equation $E_{\mathrm{LUMO/HOMO}} = -e(4.88+V_{\mathrm{redox}})$,[20] where V_{redox} is the onset potential versus ferrocene of reduction or oxidization of sensitizers. The energy offsets of LUMOs (−3.35 eV for **Z907**; −3.47 eV for **C219**) of dye molecules with respect to the titania conduction band edge (−4.00 eV)[21] provide thermodynamic driving forces for charge generation. The energy offsets of HOMOs (−4.99 eV for **Z907**; −4.96 eV for **C219**) relative to that (−4.60 eV)[19g] of iodide supply negative Gibbs energy changes for dye regeneration reaction. Through a systematic comparison on electrochemical data (see Table S1 in the Supporting

(20) Yan, Q.; Zhou, Y.; Ni, B.; Ma, Y.; Wang, J.; Pei, J.; Cao, Y. *J. Org. Chem.* **2008**, *73*, 5328.
(21) (a) Hagfeldf, A.; Grätzel, M. *Chem. Rev.* **1995**, *95*, 49. (b) Grätzel, M. *Nature* **2001**, *414*, 338.

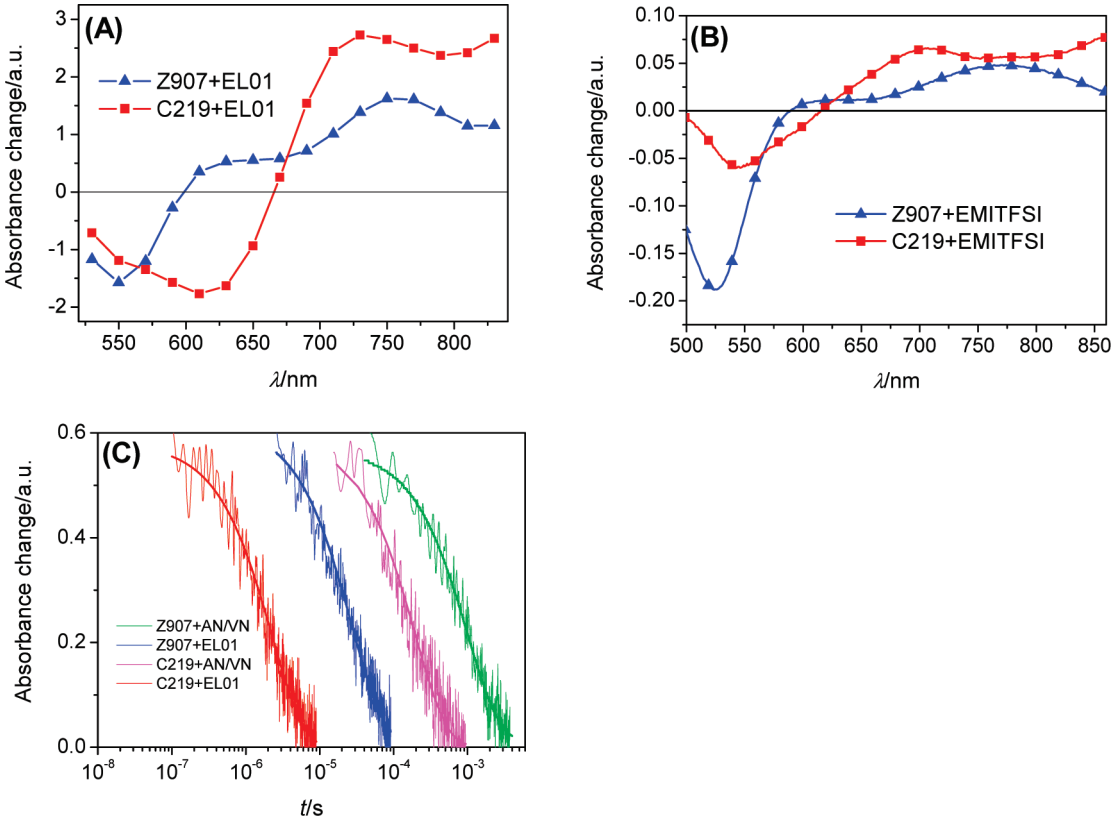

Figure 4. (A) Transient absorption changes recorded at 210 ns upon nanosecond pulsed laser excitation of dye-coated titania films immersed in **EL01**. (B) Absorption changes after applying a small positive bias to dye-coated titania films immersed in EMITFSI. (C) Time-resolved absorption traces of dye-coated titania films in the 85/15 mixed solvent of acetonitrile (AN) and valeronitrile (VN) and in **EL01**. Smooth solid lines are single exponential fits of experimental data. Absorbance changes were measured at a probe wavelength of 782 nm upon 540 nm (for **Z907**) or 606 nm (for **C219**) pulsed laser excitation (7 ns full width half-maximum pulse duration, 2 Hz repetition rate, 1.35×10^{14} photons cm^{-2} pulse fluence). Signals shown were obtained by averaging over 1600 laser shots.

Information) of all organic dyes reported by our group so far, it is clear that the **C219** dye has a relative small HOMO/LUMO gap of 1.49 eV, generally consistent with its low-energy absorption peak. The influence of π-conjugation spacer on HOMOs and LUMOs of chromophores can also be easily perceived from Table S1 in the Supporting Information.

3.2. Transient Absorption Spectra and Charge-Transfer Kinetics. A 2.5 μm thick dye-coated transparent titania film on glass slide was employed to make a dummy cell in combination with an acetonitrile electrolyte **EL01** for transient absorption spectra measurements. The absorption changes in the spectral range from 530 to 830 nm (Figure 4A) were recorded at 210 ns using a white probe light, upon nanosecond pulsed laser excitation. We assign these long-lived negative signals to the bleaching of ground-state dye molecules. In consideration of less than 30 ns photoluminescence traces of dye-coated zirconia films, we rule out any contribution from dye emission to the positive signals. At the titania/dye interface, an ultrafast charge generation from organic excitons ejects electrons into titania nanocrystals and leaves holes on dye molecules, producing oxidized dye cations. With the aid of spectroelectrochemical measurements (Figure 4B) on dye-coated film immersed in 1-ethyl-3-methylimidazolium bis(trifluoromethanesulfonyl)imide (EMITFSI), we could ascribe the positive changes in the transient absorption spectra to the electronic absorptions of oxidized dye cations. Note that the concomitant electrons in titania exhibit relatively weak absorptions throughout this spectral region ($\varepsilon_{780} = 3400\ M^{-1}\ cm^{-1}$).[22]

On the basis of transient absorption measurements, we selected a 780 nm monochromatic light to probe the kinetics of charge recombination of trapped electrons in titania with oxidized dye cations, and that of interception of oxidized dye cations by iodide ions (electron donor), i.e., dye regeneration. To a large extent the kinetic competition between these two charge-transfer channels are widely believed to determine IPCEs of DSCs, along with the yields of light absorption, electron injection, and charge collection.[23] The excitation wavelength and fluence were carefully controlled in our kinetic measurements to ensure that $\sim 1.35 \times 10^{14}$ photons cm^{-2} was absorbed by dye-coated films during every laser pulse, which is close to the light intensity of device operation. Because no electron donor is existent in the 85/15 mixture

(22) Rothenburger, G.; Fitzmaurice, D.; Grätzel, M. *J. Phys. Chem.* **1992**, *96*, 5983.
(23) (a) Tachibana, Y.; Moser, J. E.; Grätzel, M.; Klug, D. R.; Durrant, J. R. *J. Phys. Chem.* **1996**, *100*, 20056. (b) Haque, S. A.; Tachibana, Y.; Willis, R. L.; Moser, J. E.; Grätzel, M.; Klug, D. R.; Durrant, J. R. *J. Phys. Chem. B* **2000**, *104*, 538. (c) Pelet, S.; Moser, J. E.; Grätzel, M. *J. Phys. Chem. B* **2000**, *104*, 1791. (d) Wang, P.; Klein, C.; Moser, J.-E.; Humphry-Baker, R.; Cevey-Ha, N.-L.; Charvet, R.; Comte, P.; Zakeeruddin, S. M.; Grätzel, M. *J. Phys. Chem. B* **2004**, *108*, 17553.

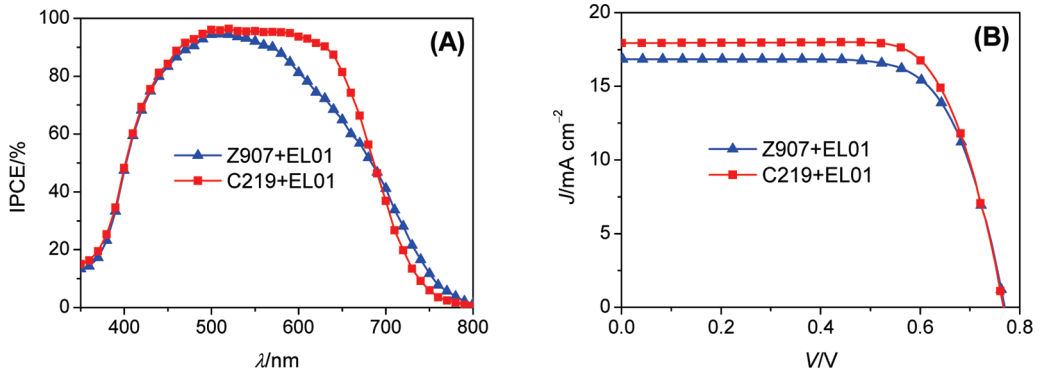

Figure 5. (A) Photocurrent action spectra of cells made from **Z907** and **C219** in combination with an acetonitrile based electrolyte **EL01**. (B) $J-V$ characteristics of cells measured under irradiation of 100 mW cm^{-2} AM1.5G sunlight. An antireflection film was adhered to cells during measurements. **EL01** is composed of 1.0 M DMII, 50 mM LiI, 30 mM I_2, 0.5 M TBY, and 0.1 M GNCS in the 85/15 mixture of acetonitrile and valeronitrile.

of acetonitrile and valeronitrile, the absorption decays reflect the kinetics of recombination of injected electrons with oxidized dye cations. The absorption traces in Figure 4C can be well-fitted by a single exponential decay function, with a lifetime (τ_b) of 194 μs for **Z907** cations and 994 μs for **C219** cations. When the dye-coated titania films are submerged in **EL01** with a high concentration of iodide ions, the decays (Figure 4C) are significantly accelerated, characteristic of a single exponential lifetime (τ_r) of 2.3 μs for **Z907** cations and that of 27.1 μs for **C219** cations. Even if the rate constants of both back-electron transfer and dye-regeneration are dissimilar in the cases of **Z907** and **C219**, the τ_b/τ_r branching ratios of over 35 for both dyes imply that at least 97% of oxidized dye cations are intercepted by electron donation from iodide, resulting in very efficient dye-regeneration and therefore high-yield net charge separation.

3.3. Photovoltaic Performance. Our previous work[24] has shown that both thickness and architecture of titania films have significant influences on efficiencies of DSCs fabricated from **EL01** and **Z907**, owing to fairly low light absorption coefficients of this dye in the whole visible and near-infrared region. However in combination with a state of the art double-layer titania film, 9.0−9.5% efficiencies can be indeed attained with **Z907** by using an acetonitrile based electrolyte.[10,24] Considerable efficiency superiorities of **C219** with respect to **Z907** were observed in our prior experiments using a thin transparent titania film. However, in this paper, we will utilize a double-layer film (7 + 5) with a 7 μm thick nanoporous layer and a 5-μm-thick scattering layer for comparisons, having an impartial evaluation on the status of metal-free organic photosensitizers relative to the standard amphiphilic ruthenium dye **Z907**, which has already been applied in the first commercial product of DSCs.[25]

As depicted in Figure 5A, IPCE maxima of both dyes are close to 95% after coating our cells with an antireflection film. If the light loss caused by reflection of smooth glass was not attenuated, ~4% lower IPCEs were observed in our measurements on thousands of cells.

Table 1. Detailed Photovoltaic Parameters[a] of DSCs with Z907 and C219 Using a Solvent-Free Ionic Liquid Electrolyte

dye	P_{in} (mW cm^{-2})	J_{sc} (mA cm^{-2})	V_{oc} (mV)	FF	η (%)
Z907	14.39	2.13	660.1	0.796	7.8
	26.14	3.80	678.0	0.784	7.7
	53.26	7.50	698.8	0.769	7.6
	100	13.34	713.0	0.752	7.2
C219	14.39	2.52	641.3	0.791	8.9
	26.14	4.47	659.1	0.783	8.8
	53.26	8.65	677.5	0.762	8.4
	100	14.96	693.0	0.736	7.6

[a] The spectral distribution of our light resource simulates AM 1.5G solar emission with a mismatch less than 5%. Lights at different intensities were obtained by attenuating the AM1.5G full sunlight with a set of neutral meshes. Incident power intensity, P_{in}; short-circuit photocurrent density, J_{sc}; open-circuit photovoltage, V_{oc}; fill factor, FF; total power conversion efficiency, η. Cell area tested with a metal mask: 0.158 cm^2. An antireflection film was adhered to testing cells during measurements. The composition of solvent-free ionic liquid electrolyte **EL02** is as follows: DMII/EMII/EMITCB/I_2/TBP/GNCS (molar ratio: 12/12/16/1.67/3.33/0.67).

Notably, the photocurrent action spectrum of **C219** departures evidently from the thin-film absorption spectrum (see Figure S3 of the Supporting Information), featuring a broad plateau from 500 to 590 nm because of close to unity light-harvesting by the double-layer cell architecture in this spectral region. It is valuable to note that the infrared IPCEs of **C219** are still low in comparison with that of **Z907**, highlighting the future necessary efforts on narrowing the energy gap of metal-free organic dyes. $J-V$ characteristics were further measured under irradiation of AM1.5G full sunlight and presented in Figure 5B. The short-circuit photocurrent density (J_{sc}), open-circuit photovoltage (V_{oc}), and fill factor (FF) of a cell made from **Z907** are 16.84 mA cm^{-2}, 773 mV, and 0.715, respectively, yielding an overall conversion efficiency (η) of 9.3%, well-consistent with previously reported data.[10,24] In contrast, photovoltaic parameters (J_{sc}, V_{oc}, FF, and η) of the **C219** cell are 17.94 mA cm^{-2}, 770 mV, 0.730, and 10.1%. Two batches of 10 cells show an efficiency range from 10.0 to 10.3%. The improved photocurrent of **C219** relative to **Z907** is in good accord with the preceding IPCE measurements. This is the first time greater than 10% efficiency has been reached by dye-sensitized solar cells with a nonruthenium photosensitizer.[4,19] We remark that under the same

(24) Cao, Y.; Bai, Y.; Yu, Q.; Cheng, Y.; Liu, S.; Shi, D.; Gao, F.; Wang, P. *J. Phys. Chem. C* **2009**, *113*, 6290.
(25) http://www.g24i.com.

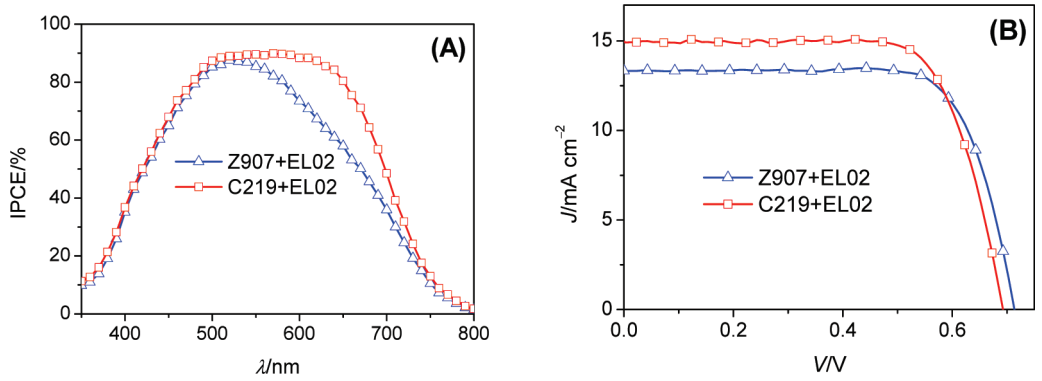

Figure 6. (A) Photocurrent action spectra of cells made from **Z907** and **C219** in combination with a solvent-free ionic liquid electrolyte **EL02**. (B) $J-V$ characteristics of cells measured under irradiation of 100 mW cm^{-2} AM1.5G sunlight. An antireflection film was adhered to cells during measurements. The composition of solvent-free ionic liquid electrolyte **EL02** is as follows: DMII/EMII/EMITCB/I_2/TBP/GNCS (molar ratio: 12/12/16/1.67/3.33/0.67).

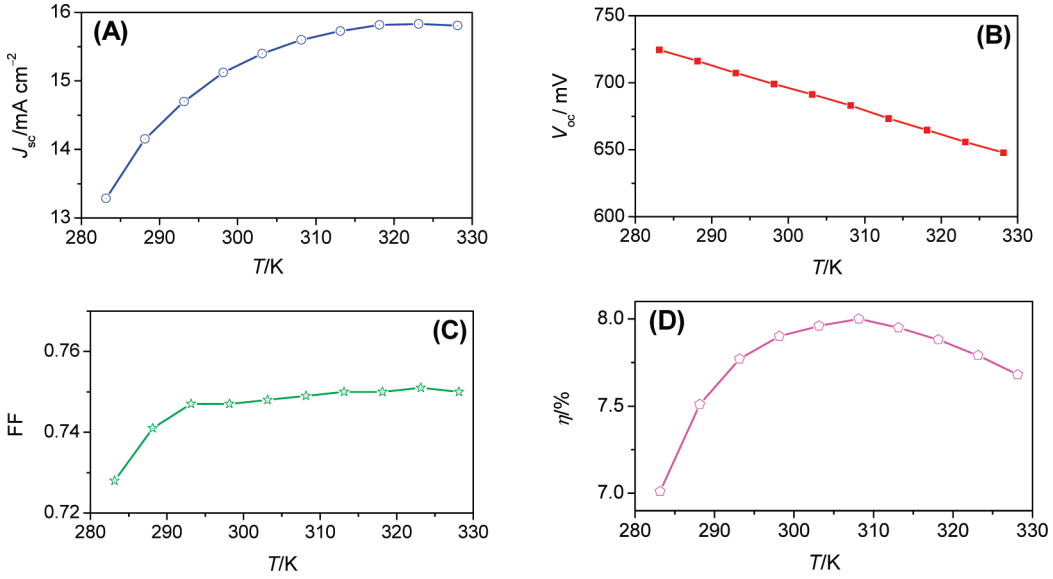

Figure 7. Temperature-dependent photovoltaic parameters of a DSC made with **C219** in combination with a solvent-free ionic liquid electrolyte **EL02**.

conditions, a reference cell with a new generation high-absorption ruthenium dye **C106** shows an efficiency of 11.3%,[24] still leaving the performance of organic dyes behind. Photovoltaic data on all other metal-free organic dyes[19] reported by our group are also collected in Table S1 in the Supporting Information for a preliminary understanding. Note that these comparisons must be taken very carefully because several solvents for the dye bath and different cheno concentrations, staining time, washing solvents, and even the base tetra-*n*-butylamonium hydroxide have been applied in our device fabrication, which have a significant influence on cell parameters. Unfortunately, we do not find a very good rationale during optimization of dye staining, which should be closely related to the dye-uploaded amount and perhaps dye-anchoring mode. We think that the latter could have a strong impact on multichannel charge transfer kinetics. The complicated interfacial chemistry and intrinsic physics behind these need to be fully addressed in some further joint studies with advanced scanning probe microscopic, computational, photophysical, and optoelectronic methods. Whatever, widening the spectral response of DSCs is the first critical step to significantly improve cell performance close to the challenging 15% efficiency, because presently the main limiting factor on the inferior efficiency of DSCs with respect to crystalline solar cells is a much lower photocurrent owing to an insufficient light-harvesting of photosensitizers.

We believe that a substantial improvement in device efficiency is still desirable to lower the cost per kilowatt-hour of energy supply with dye-sensitized solar panels in the near future. Nevertheless, stable, low-cost, flexible, and lightweight DSCs based on a plastic matrix are attractive, even if their efficiencies are moderate, i.e., in the 5−10% range. However, for these devices, the use of organic solvents is likely prohibitive as they would permeate across the polymeric cell walls. Thus we also studied the performance of **C219** and **Z907** in conjunction with a solvent-free ionic liquid electrolyte (see Figure 6). In contrast to the acetonitrile cells, a slight decrease in IPCE maxima (~90%) was noted for the ionic liquid cells, apart from a clear diminishment in the blue region due to a high concentration of triiodide in our ionic liquid electrolyte

EL02. Note that the light absorption by triiodide does not contribute to photocurrents in DSCs. Moreover, in any part of the whole spectrum the **Z907** cell with **EL02** does not exhibit higher IPCEs anymore than the **C219** cell. This was further rationalized by the electronic absorption measurements of dummy cells. As shown in Figure S3 of the Supporting Information, the **C219**-coated film immersed in **EL02** can harvest more low-energy photons than that in **EL01**, probably because of the sensitive response of **C219** to the dielectric change of these two electrolytes. Photovoltaic parameters (J_{sc}, V_{oc}, FF, and η) of the **C219** cell with a solvent-free ionic liquid electrolyte under the AM 1.5G full sunlight (100 mW cm^{-2}) are 14.96 mA cm^{-2}, 693 mV, 0.736, and 7.6%, respectively. In contrast, the **Z907** cell has an efficiency of 7.2% at the same condition. At low light intensities of 14.39 mW cm^{-2} and 26.14 mW cm^{-2} attenuated by a set of metal meshes, very impressive efficiency of 8.9% and 8.8% has been reached with **C219**. This is very favorable for the practical indoor application of flexible devices, which are frequently operated under reduced light intensities and for which ionic liquids are the electrolytes of choice.[26] We have noted that the measured photocurrent densities under the full sunlight for both cells are significantly lower than the overlap integral currents of the IPCE curves with the standard AM1.5G solar emission spectrum. As listed in Table 1, there is a clear nonlinear dependence of short-circuit photocurrent on light intensity, implying that photocurrents of our ionic liquid cells with **Z907** and **C219** could be limited by the slow transport of redox mediators in this viscous electrolyte. Moreover, a solvent-free DSC with **C219** as sensitizer exhibits an excellent stability (Figure S4 of the Supporting Information), keeping more than 93% of its initial efficiency after 1000 h of aging under the full sunlight soaking at 60 °C.

For the outdoor application of dye-sensitized solar cells, the cell may operate at various temperatures. Thereby, we also measured $J-V$ characteristics of a solvent-free ionic liquid cell made from **C219** at various temperatures. As presented in Figure 7A, the short-circuit photocurrent augments with temperature from 10 to 45 °C but saturates upon a further temperature improvement. Our electrical impedance measurements[27] have shown that the electron diffusion length (L_n) is shortened at a high temperature (Figure 8A), indicating that the increase of photocurrent with temperature is probably not related to a better charge collection yield. In addition, we did not observe a light-harvesting enhancement for cells at a high temperature. At the moment, we could not rule out whether the temperature-dependent photocurrent tendency is also related to the net charge generation yield, which needs to be addressed in our future studies.

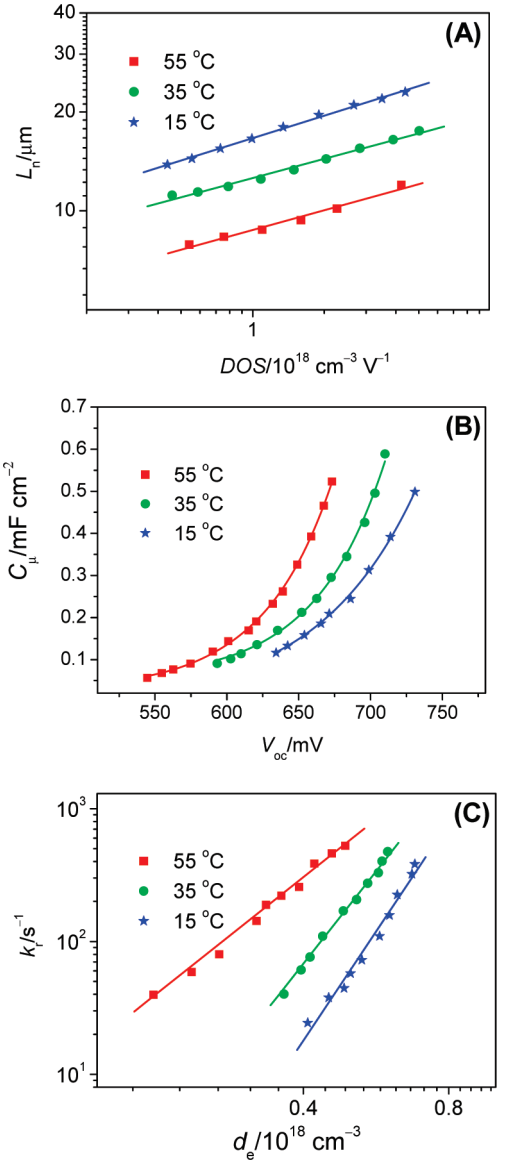

Figure 8. Temperature-dependent (A) electron diffusion length versus density of states (*DOS*) measured with electrical impedance spectroscopy, (B) chemical capacitance, and (C) charge recombination constant derived from measurements on transient photovoltage and photocurrent decays.

As the viscosity of **EL02** becomes low with temperature, the dependence of photocurrent on temperature could be ascribed to the limit of electrolyte transport at low temperatures. Furthermore, poor fill factors were observed at 10 and 15 °C because of the relatively large cell serial resistances, including electrolyte diffusion resistances, charge-transfer resistances on the counter electrode, and electron transport resistances in the semiconducting titania film. The overall power conversion efficiencies at temperatures from 10 to 55 °C are over 7%, with a maximum of 8.0% at 35 °C due to a trade-off among J_{sc}, FF, and V_{oc}.

To comprehend the adverse effect of raising temperature on cell photovoltage, we resorted to the transient photoelectrical decay technique[28] to measure interfacial chemical capacitance (C_μ) and charge recombination kinetics. As presented in Figure 8B, at a set of temperatures the capacitance closely related to surface states

(26) Shi, D.; Pootrakuchote, N.; Li, R.; Guo, J.; Wang, Y.; Zakeeruddin, S. M.; Grätzel, M.; Wang, P. *J. Phys. Chem. C* **2008**, *112*, 17046.
(27) (a) Bisquert, J. *J. Phys. Chem. B* **2002**, *106*, 325. (b) Bisquert, J. *Phys. Chem. Chem. Phys*. **2003**, *5*, 5360. (c) Bisquert, J. *Phys. Chem. Chem. Phys*. **2008**, *10*, 49.

under the conduction band edge of titania increases exponentially with the enlargement of V_{oc}, which was generated by applying a gradually enhanced white light intensity. At a given V_{oc}, the apparently higher C_μ at a higher temperature could be attributed to more deep surface states because the calculated equilibrium potential of **EL02** at 55 °C has a less than 10 mV negative shift relative to that at 10 °C. As shown in Figure 8C, at a given electron density (d_e) the charge recombination rate (k_r) becomes fast with temperature, which could be mainly caused by the enhanced diffusion coefficients of triiodide anions and electrons in the titania film, implying a bimolecular interfacial recombination process. It is likely that at a high temperature, deep electron-traps and fast interfacial charge recombination kinetics together lead to a decreased open-circuit photovoltage.

4. Conclusions

To summarize, we have prepared a high molar absorption coefficient organic push−pull dye featuring a binary conjugated spacer of ethylenedioxythiophene and dithienosilole, apart from the blocks of a lipophilic alkoxy-substituted triphenylamine and a hydrophilic cyanoacrylic acid. On the basis of this amphiphilic photosensitizer and a volatile electrolyte, we have set a new benchmark of 10.0−10.3% efficiency measured at the AM1.5G conditions for dye-sensitized solar cells with nonruthenium dyestuffs. This achievement should considerably stimulate further efforts on energy-level engineering of organic chromophores, catching up with the high performance of ruthenium dyes. More importantly, a solvent-free ionic liquid cell based on this new dye has achieved a high efficiency of 8.9% under a low light intensity of 14.39 mW cm^{-2}, making it very promising for the practical indoor application of flexible dye-sensitized solar cells. We are now systematically optimizing electrolyte compositions and device architectures to explore the full potential of this encouraging organic sensitizer. Systematic studies on the intrinsic role of conjugated spacers on multichannel charge transfer kinetics and surface states of titania nanocrystals are needed to shed light on the structure−activity relationship for the future development of more efficient photosensitizers.

Acknowledgment. The National Key Scientific Program (2007CB936700), the National Science Foundation of China (50973105 and 50773078), the CAS Knowledge Innovation Program (KGCX2-YW-326), and the CAS Hundred Talents Program are acknowledged for financial support. M.Z. thanks the State Key Laboratory of Theoretical and Computational Chemistry, Jilin University for the computational resources. We are grateful to Dyesol for supplying the scattering paste and EMITCB, and to DuPont Packaging and Industrial Polymers for supplying the Bynel film.

Supporting Information Available: ATR-FTIR spectrum, square-wave voltammogram, additional spectral, and photovoltaic data (PDF). This material is available free of charge via the Internet at http://pubs.acs.org.

(28) (a) O'Regan, B. C.; Lenzmann, F. *J. Phys. Chem. B* **2004**, *108*, 4342. (b) O'Regan, B. C.; Scully, S.; Mayer, A. C.; Palomares, E.; Durrant, J. *J. Phys. Chem. B* **2005**, *109*, 4616. (c) O'Regan, B. C.; Durrant, J. R. *J. Phys. Chem. B* **2006**, *110*, 8544. (d) Bailes, M.; Cameron, P. J.; Lobato, K.; Peter, L. M. *J. Phys. Chem. B* **2005**, *109*, 15429. (e) Kopidakis, N.; Neale, N. R.; Frank, A. J. *J. Phys. Chem. B* **2006**, *110*, 12485. (f) Walker, A. B.; Peter, L. M.; Lobato, K.; Cameron, P. J. *J. Phys. Chem. B* **2006**, *110*, 25504. (g) Quintana, M.; Edvinsson, T.; Hagfeldt, A.; Boschloo, G. *J. Phys. Chem. C* **2007**, *111*, 1035.